NANO LETTERS

pubs.acs.org/NanoLett Letter

Observation of Coexisting Weak Localization and Superconducting Fluctuations in Strained $Sn_{1-x}In_xTe$ Thin Films

Jiashu Wang,* William Powers, Zhan Zhang, Michael Smith, Bradlee J. McIntosh, Seul Ki Bac, Logan Riney, Maksym Zhukovskyi, Tatyana Orlova, Leonid P. Rokhinson, Yi-Ting Hsu, Xinyu Liu, and Badih A. Assaf*

Cite This: https://doi.org/10.1021/acs.nanolett.1c04370 Read Online

ACCESS | Metrics & More | Article Recommendations | Supporting Information

ABSTRACT: Topological superconductors have attracted tremendous excitement as they are predicted to host Majorana zero modes that can be utilized for topological quantum computing. Candidate topological superconductor $Sn_{1-x}In_xTe$ thin films ($0 < x < 0.3$) grown by molecular beam epitaxy and strained in the (111) plane are shown to host quantum interference effects in the conductivity coexisting with superconducting fluctuations above the critical temperature T_c. An analysis of the normal state magnetoresistance reveals these effects. A crossover from weak antilocalization to localization is consistently observed in superconducting samples, indicating that superconductivity originates dominantly from charge carriers occupying trivial states that may be strongly spin−orbit split. A large enhancement of the conductivity is observed above T_c, indicating the presence of superconducting fluctuations. Our results motivate a re-examination of the debated pairing symmetry of this material when subjected to quantum confinement and lattice strain.

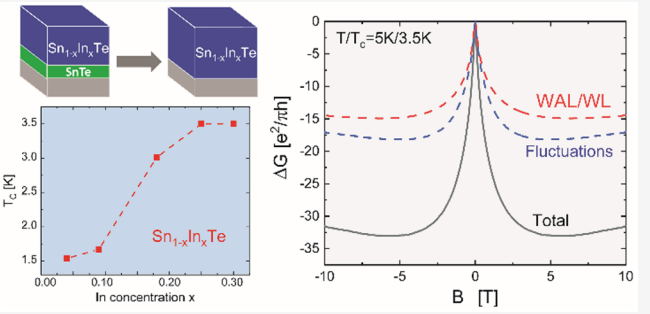

KEYWORDS: *Superconductivity, thin films, topological insulator, magnetoresistance*

Nontrivial topology in the electronic band structure leads to unique properties in various materials that include insulators, semimetals, magnets, and superconductors.[1−4] In particular, topological superconductors (TSCs) can have a gapped bulk, accompanied by gapless boundary states dubbed Majorana boundary modes that have possible applications in quantum computing.[5] This greatly motivates the current interest in TSCs. TSCs can arise in materials that are topologically nontrivial and superconducting.[6] Materials proven to be intrinsic TSCs are rare but candidates include $Cu_xBi_2Se_3$,[7,8] UTe_2,[9] UPt_3,[10] and $Sn_{1-x}In_xTe$. Alternatively, one can achieve TSCs employing the proximity effect;[11] by building heterostructures of topological insulators (TIs) and conventional superconductors, one introduces superconductivity into TIs.[12−14]

SnTe is a topological crystalline insulator (TCI).[15,16] It hosts four Dirac cones protected by crystal mirror symmetry on its (111) surface.[17,18] $Sn_{1-x}In_xTe$ can become superconducting while maintaining its topological surface states when alloyed with In.[19−23] However, the nontrivial character of superconductivity in $Sn_{1-x}In_xTe$ remains debated, and several recent experiments could not reveal the presence of odd pairing or Majorana modes.[24−28] Regardless of whether it is intrinsically topological, $Sn_{1-x}In_xTe$ is one of the few superconductors that are epitaxially compatible with TCIs and can be used in proximity effect heterostructures to achieve the TSC.

Previous research on $Sn_{1-x}In_xTe$ was focused on single crystals. The growth and analysis of $Sn_{1-x}In_xTe$ thin films are necessary to search for boundary Majorana modes using device-based schemes. Thin films also enable material tuning knobs beyond those possible for single crystals such as confinement, strain, and interfacial effects. In thin films, quantum coherent corrections to the conductivity that are useful to quantify spin−orbit splitting effects are enhanced.[29] Moreover, in the case of superconductors confinement enhances quantum coherent corrections due to superconducting fluctuations[30,31] above the critical temperature T_c, which could provide a novel route to put to test the order parameter symmetry.[32,33] The MBE growth of $Sn_{1-x}In_xTe$[34] was recently developed on InP substrates but measurements involving the

Received: November 12, 2021
Revised: January 1, 2022

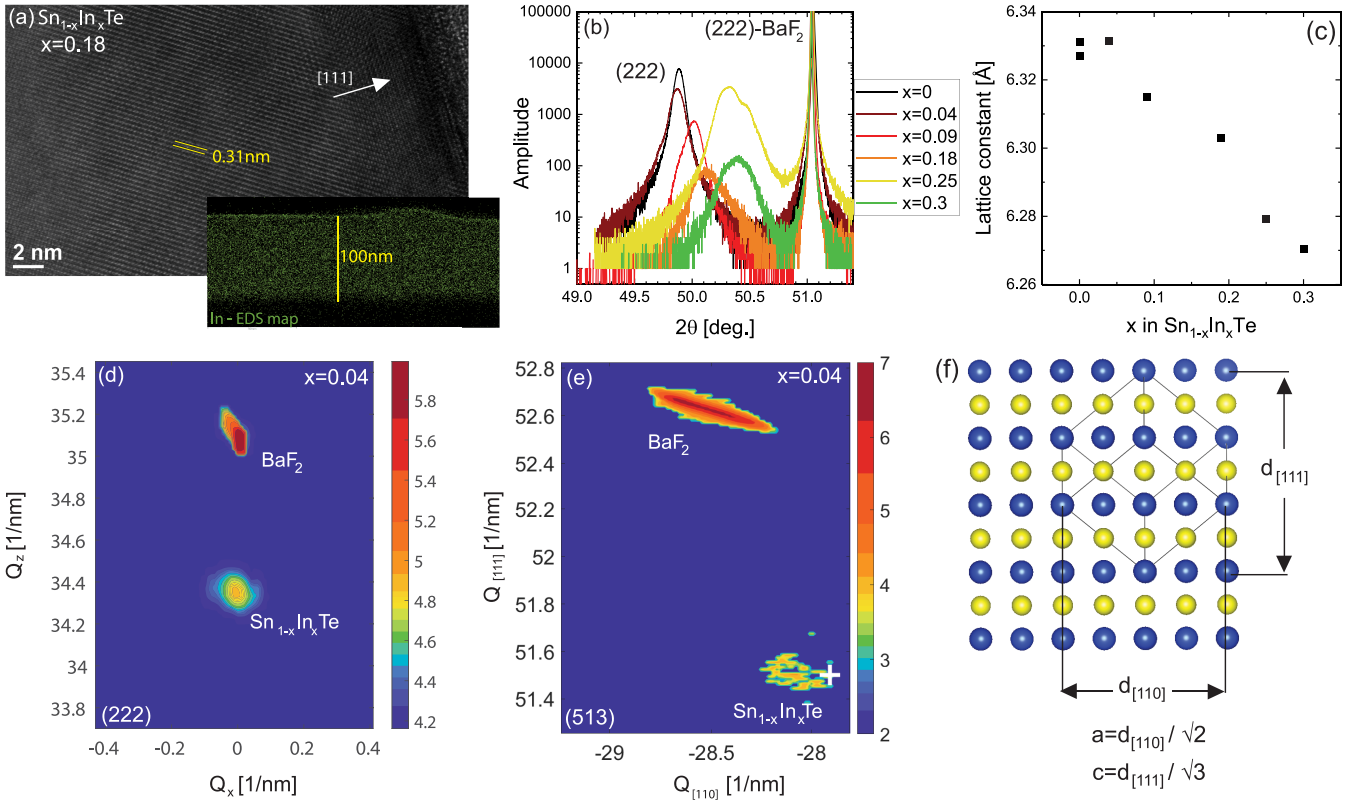

Figure 1. (a) Transmission electron microscope image of a $Sn_{1-x}In_xTe$ (x = 0.25) thin film. Inset shows an elemental mapping of the energy dispersive X-ray emission line, showing a homogeneous distribution within the instrument resolution. (b) X-ray diffraction scan about the (222) Bragg peak of films having $0 < x < 0.3$. (c) Lattice constant obtained in the (111) direction versus x. (d) RSM around (222) substrate and layer peaks. (e) RSM about the (513) peaks. The white cross corresponds to the peak expected from a relaxed cubic structure with $c = a$. (f) Schematic of a (111) oriented film showing a and c lattice constants obtained from the [110] and [111] lattice spacing, respectively.

effects of confinement on the superconducting and normal state properties of $Sn_{1-x}In_xTe$ are yet to be carried out.

Here, we report structural and electrical measurements on strained thin films of $Sn_{1-x}In_xTe$ ($0.04 < x < 0.3$) grown by MBE on BaF_2 (111) that reveal remarkable differences compared to single crystals. The films host rhombohedral strain along the (111) planes that alters the crystal symmetry. They are all superconducting for $x > 0.04$ but also exhibit strongly enhanced quantum coherent corrections to the conductivity that unravel important properties of the normal state. In the normal state, quantum interference effects and superconducting fluctuations coexist. A crossover from weak antilocalization (WAL) to weak localization (WL) in superconducting $Sn_{1-x}In_xTe$ indicates that electrons from trivial bulk states play a dominant role in the superconducting state. However, the observation of WAL at low magnetic field indicates the presence of bulk spin−orbit splitting possibly due to Rashba splitting whose origin is discussed. Close to but above T_c, a significant enhancement of the conductivity and a strong negative magnetoconductance indicate the presence of Maki−Thompson superconducting fluctuations. The absence of a signature of fluctuations in the Meissner effect corroborates this interpretation. Our realization of $Sn_{1-x}In_xTe$ thin films and the observation of the WAL and fluctuations shed a new light on the properties of this material, which is likely to change under the impact of quantum confinement and lattice strain.

Thin film of $Sn_{1-x}In_xTe$ ($0.04 < x < 0.3$) are grown by molecular-beam epitaxy (MBE) on BaF_2 (111) substrate. We initially deposit a buffer layer of SnTe (<40 nm) to start the nucleation of the layer. We then co-deposit Sn, In, and Te from elemental cells. Throughout the growth, we vary the cell temperature as well as the relative growth time of SnTe and $Sn_{1-x}In_xTe$ layers to control composition (see Supporting Information). Layers of $Sn_{1-x}In_xTe$ with $0 < x < 0.3$ are obtained.

The In atoms are found to diffuse into the SnTe buffer almost regardless of composition and buffer layer thickness. Transmission electron microscopy (TEM) measurements and an energy dispersive X-ray (EDX) map of the In distribution performed at room temperature on a sample having x = 0.18 confirm this. They are shown in Figure 1a. The image yields well resolved atomic layers confirming the good crystalline quality of the films. The EDX measurements show a uniform In distribution within the resolution of the instrument (∼±2%). The diffusion of In during the growth thus leads to a homogeneous $Sn_{1-x}In_xTe$ layer with a thickness of 100 nm.

X-ray diffraction scans of the (222) Bragg peaks of various $Sn_{1-x}In_xTe$ films are shown in Figure 1b. The peak position shifts to higher angle with increasing In, indicating a decrease of the lattice constant as shown in Figure 1c. This agrees with previous reports on single crystals and thin films.[34,35]

The slight lattice mismatch between $Sn_{1-x}In_xTe$ (∼6.33−6.26 Å) and BaF_2 (6.196 Å) warrants a thorough investigation

https://doi.org/10.1021/acs.nanolett.1c04370
Nano Lett. XXXX, XXX, XXX−XXX

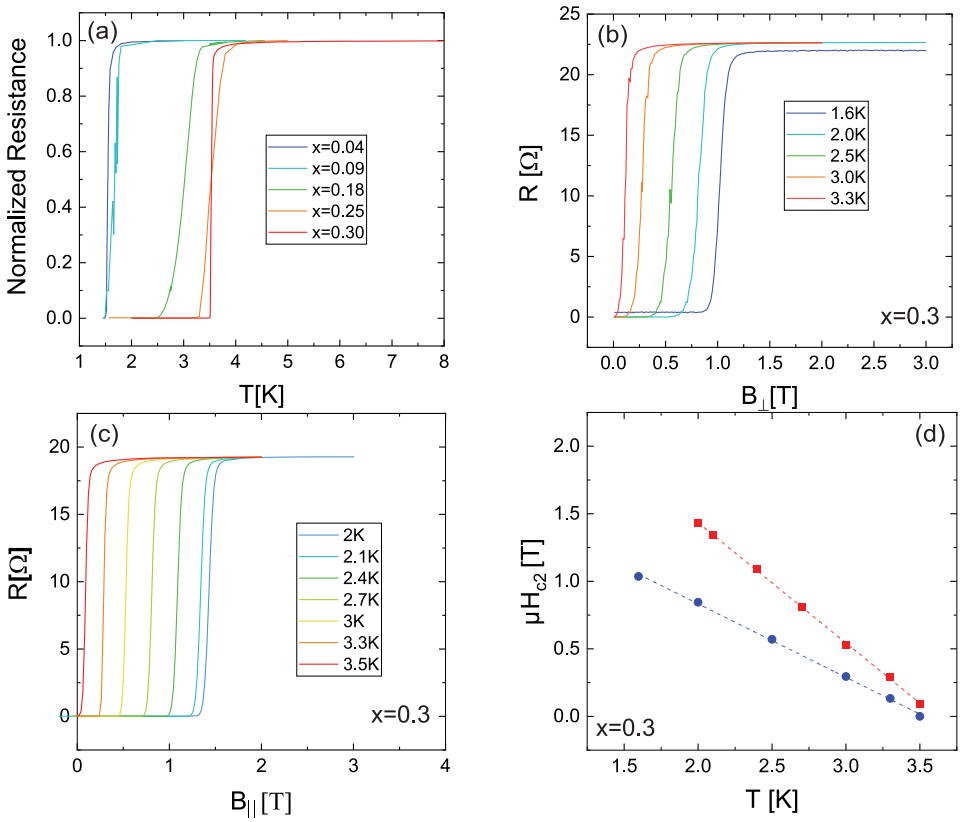

Figure 2. (a) Dependence of T_c on In concentration. (b) Magnetic field dependence of resistivity in the superconducting regime for $Sn_{0.7}In_{0.3}Te$ at different temperatures for a field applied perpendicular to the sample plane. (c) Same as (b) but for field applied in the plane perpendicular to the current. (d) Temperature dependence of critical field applied in-plane and out-of-plane. Points are taken at half of the normal state resistance. Dashed lines are fitting curves using Ginzburg−Landau theory.

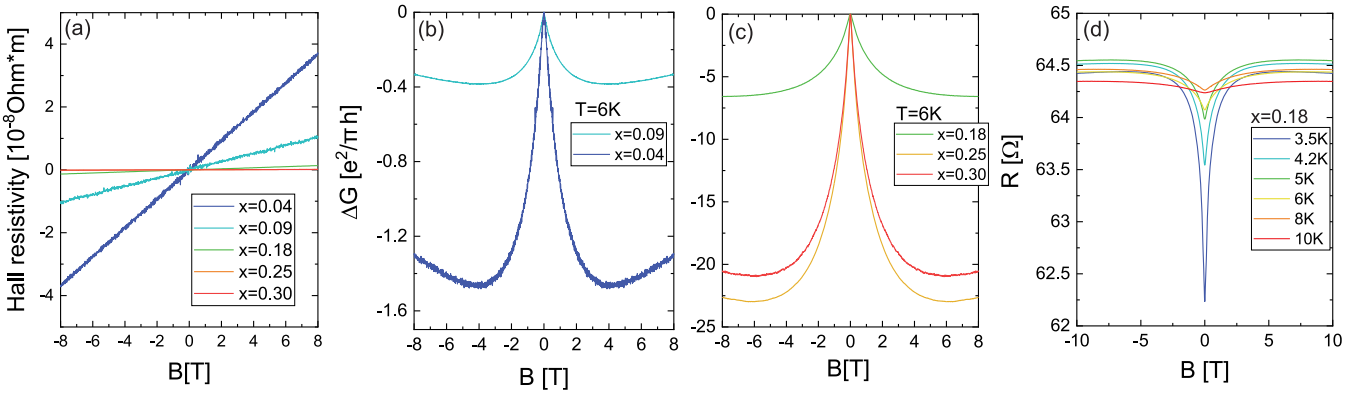

Figure 3. (a) Hall resistivity for samples with different In concentration. As the In content increases the slope of the line gradually decreases. (b,c) Magneto-conductance of samples with different In concentration at 6 K, in the normal state. (d) Resistance of sample $x = 0.18$ versus magnetic field at different temperatures.

of the in-plane lattice parameter. Thus, high-resolution X-ray diffraction is performed around the (222) and (513) Bragg peaks. The resulting reciprocal maps (RSMs) for $x = 0.04$ are shown in Figure 1d,e, respectively. The analysis of the RSMs yields the lattice constant c and a, respectively, in the directions parallel and perpendicular to the [111] growth direction. Here, we define $c = d_{[111]}/\sqrt{3}$ and $a = d_{[110]}/\sqrt{2}$ where $d_{[hkl]}$ represents the lattice spacing in the $[hkl]$ direction. From Figure 1d, we use the (222) Bragg peak to obtain $c = 6.331$ Å ($\pm$<0.001). From Figure 1e, the (513) peak allows us to find $a = 6.290 \pm 0.003$ Å (the uncertainty spans the width of the peak and is thus an overestimation). The layer is thus compressively strained in the (111) plane and tensile-strained out-of-plane along the growth axis, breaking cubic crystalline symmetry (Figure 1f). Similar data for $x = 0.09$ is shown in Supporting Information. In Figure 1e, a cross locates the peak expected from an unstrained layer (i.e., $a = c$) on the RSM. The experimental Bragg peak is broad but evidently located left of the cross. Thus, even at 100 nm, the layer remains under stress and $c > a$.

Electrical transport measurement are performed from 1.5 K to 15 K using the standard 5-probe method. Gold wires are attached to the film using conducting silver paste. All In-containing samples with $x \geq 0.04$ exhibit a superconducting

https://doi.org/10.1021/acs.nanolett.1c04370
Nano Lett. XXXX, XXX, XXX−XXX

regime at low temperature. As we increase the In concentration, the critical temperature T_c gradually rises from 1.5 K to 3.5 K, as shown in Figure 2a, in agreement with previous work.[34,36,37,35,21] Figure 2b,c plots the sample resistance versus magnetic field applied out-of-plane and in-plane, respectively. The plots show several temperatures below T_c. The upper critical field H_{c2}, defined as the midpoint between the normal state resistance and 0, is extracted and plotted versus temperature in Figure 2d. The plots show the anisotropy between out-of-plane and in-plane directions and a quasi-linear relationship of H_{c2} with respect to temperature for both directions. This indicates that the superconducting state is quasi-3D. The two curves can be well fit by the 3D Ginzburg–Landau theory

$$\mu_0 H_{c2}^{i} = \mu_0 H_{c2}^{i}(0)\left[1 - \frac{T}{T_c}\right]$$

where $H_{c2}^{i}(0) = H_{c2}^{\perp}{}^{\parallel}(0)$ are the critical fields at $T = 0$ K, found to be $H_{c2}^{\perp}(0) = 1.92T$ and $H_{c2}^{\parallel}(0) = 3.27T$. This is below the Pauli limit $B_P \approx 1.85 \times T_C \approx 6.5T$. Using the relation $\mu_0 H_{c2}^{\perp}(0) = \frac{\Phi_0}{2\pi\xi_{ab}^2}$ and $\mu_0 H_{c2}^{\parallel}(0) = \frac{\Phi_0}{2\pi\xi_{ab}\xi_c}$, where $\Phi_0 = \frac{h}{2e}$ is the flux quantum, we can estimate the superconducting coherence length ξ_{ab} (in plane) and ξ_c (out of plane). The extracted values are 12.9 and 7.6 nm, respectively. Their value is smaller than the thickness of the film (100 nm), evidencing a quasi-3D superconductivity.

Figure 3 summarizes the transport measurements carried out in the normal state. The Hall effect, shown in Figure 3a, reveals a decreasing Hall constant with increasing In, suggesting that In is an acceptor. However, the carrier density calculated based on this exceeds 10^{23} cm^{-3} for $x \geq 0.18$ which is unrealistic as it exceeds the atomic density. This corresponds to a Hall coefficient ~0.0001 cm^3/C. We suspect that the small Hall coefficient can be caused by the coexistence of holes and electrons that both have a low mobility as previously discussed for single crystals.[38] In this situation, the Hall resistivity in the Drude model follows

$$\rho_{xy} \approx \frac{(n_h - n_e)}{e(n_h + n_e)^2}B$$

where $n_{e,h}$ is the carrier density of electrons/holes. Thus, the effective carrier density calculated from the Hall slope can be unreasonably high if $n_h - n_e$ is small. As we increase In, n_e increases thus gradually lowering the Hall coefficient. From this, we conclude that In acts as an electron donor, possibly generating an impurity band near the Fermi level. Several recent works report similar observations.[23,38] This impurity band is believed to play an essential role in the superconductivity of this material.[19]

In the normal state, for all superconducting samples a cusp at lower perpendicular field followed by a negative magnetoresistance at intermediate field is observed as shown in Figure 3b,c. Such a behavior can generally be attributed to a crossover from WAL to WL, both caused by quantum interference corrections to the conductivity. At low field, Figure 3d shows a decreasing resistance as the sample is cooled down, indicating that WL is not dominant. The 2D Hikami–Larkin–Nagaoka (HLN) model is commonly used to explain WAL and WL and is given by[29,39]

$$\Delta G(B) = -\frac{Ne^2}{2\pi h}\left[\psi\left(\frac{B_\varphi}{B} + \frac{1}{2}\right) - \ln\left(\frac{B_\varphi}{B}\right)\right] - \frac{Ne^2}{\pi h}\left[\psi\left(\frac{B_{SO} + B_e}{B} + \frac{1}{2}\right) - \ln\left(\frac{B_{SO} + B_e}{B}\right)\right] + \frac{3Ne^2}{2\pi h}\left[\psi\left(\frac{\left(\frac{4}{3}\right)B_{SO} + B_\varphi}{B} + \frac{1}{2}\right) - \ln\left(\frac{\left(\frac{4}{3}\right)B_{SO} + B_\varphi}{B}\right)\right] \quad (1)$$

where ψ is the digamma function, $B_i = \frac{\hbar}{4eL_i^2}$, L_φ is the phase coherence length, L_{SO} is the spin–orbit relaxation length, and L_e is the elastic scattering length. N represents the total number of channels, usually representing subband or valley degeneracy. For samples with low mobility and short elastic scattering length, $B_e \gg B_{SO}$, B_φ and the middle term containing B_e in eq 1 is negligible. In TCIs and PbTe, 4-fold valley degeneracy can enhance the (anti)localization effect by increasing channel numbers ($N \approx 4$).[40,41]

However, the absolute value of the negative magnetoconductance cusp is high and can reach $10e^2/h$, as shown in Figure 3c. There is a 20-fold enhancement of its magnitude for $x > 0.18$ which cannot be simply attributed to the WAL effect that typically yields corrections on the order of $1e^2/h$.[29,41−44] This is especially the case at low temperature below 6 K ($T/T_c < 2$) as seen for $x = 0.18$ in Figure 3d. Therefore, superconducting fluctuations must be contributing to the conductance above T_c. We consider three common terms to describe fluctuations. (i) The Aslamazov-Larkin (AL) fluctuations are directly connected to the fluctuating cooper pairs and dominate at T very close to T_c ($(T - T_c)/T_c \ll 1$).[45,46] (ii) The Maki–Thompson (MT) fluctuations originate from the coherent interaction of electrons with fluctuating Cooper pairs.[30,47,48] (iii) The density-of-states (DOS) term arises from the changing single-particle density of states due to the involvement of carriers in fluctuation pairing.[49,50] As the magnetic field increases, the fluctuations are suppressed, leading to negative magneto-conductivity from AL and MT and a positive contribution from DOS. In 2D, that is, when $\left(\frac{\xi_c}{t}\right)^2 < (T - T_c)/T_c$ as in our case, the conductance correction from the MT term is given by

$$\Delta G_{MT}(T, H) = -\frac{e^2}{\pi h}\beta_L\left(\frac{T}{T_c}\right)\left[\Psi\left(\frac{1}{2} + \frac{B_\varphi}{B}\right) - \ln\left(\frac{B_\varphi}{B}\right)\right] \quad (2)$$

$\beta_L\left(\frac{T}{T_c}\right)$ is Larkin's electron–electron interaction strength parameter tabulated in ref.[30] We utilize the HLN model in its 2D form despite our films being 100 nm thick. The MT term differs from the HLN model only by a prefactor (Supporting Information S3).[29,44,49,51−55] Our fitting formula is obtained by combining all possible contributions from fluctuations with WL[56−58]

$$\Delta G(B, T) = -\frac{\left(N + \beta_L\left(\frac{T}{T_c}\right)\right)e^2}{2\pi h}\left[\psi\left(\frac{B_\varphi}{B} + \frac{1}{2}\right) - \ln\left(\frac{B_\varphi}{B}\right)\right] + \frac{3Ne^2}{2\pi h}\left[\psi\left(\frac{4B_{SO}/3 + B_\varphi}{B} + \frac{1}{2}\right) - \ln\left(\frac{4B_{SO}/3 + B_\varphi}{B}\right)\right] + \Delta G_{AL}(B, T) + \Delta G_{DOS}(B, T) \quad (3)$$

https://doi.org/10.1021/acs.nanolett.1c04370
Nano Lett. XXXX, XXX, XXX−XXX

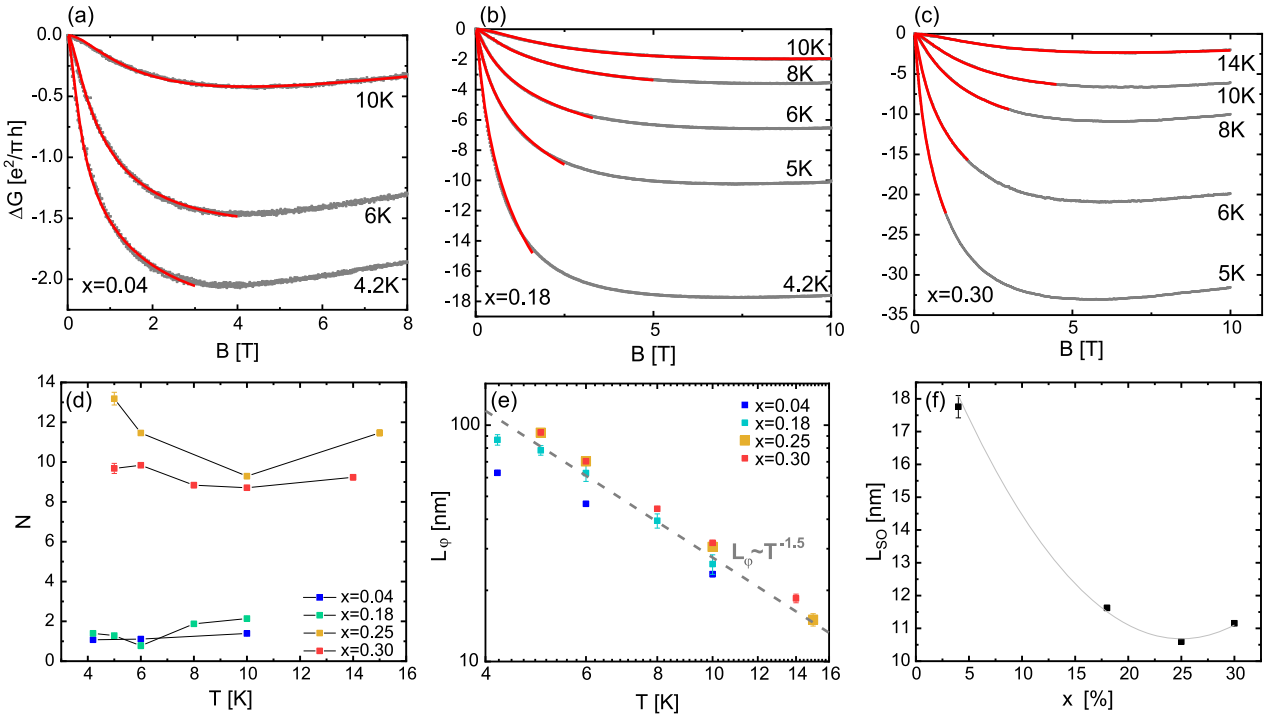

Figure 4. Fitting results for superconducting samples. (a−c) Show the fitting curves using eq 3 for $x = 0.04$, $x = 0.18$, and $x = 0.30$, respectively. (d) Channel number and (e) coherence length versus temperature for samples with different In concentration. (f) Spin−orbit scattering length versus In content x.

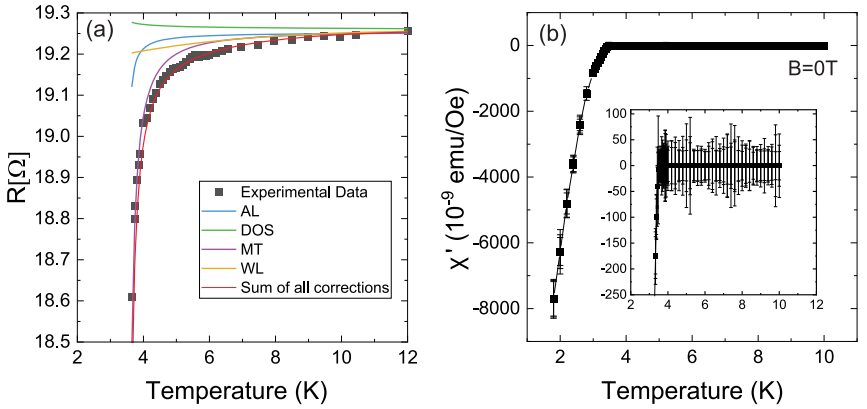

Figure 5. (a) Plot of resistance versus temperature and comparison with different the AL, MR, and DOS and WAL contributions near T_c. Almost all parameters are taken from magneto-conductance fitting result. Detailed expression can be found in Supporting Information. (b) AC susceptibility versus temperature for $x = 0.3$.

Notice that eq 3 only has N, B_φ, and B_{SO} as fitting parameters. B_φ is temperature dependent, and B_{SO} should be temperature independent. ΔG_{AL} and ΔG_{DOS} do not contain any fit parameters and are shown to have a negligible contribution (see Supporting Information S3) compared to MT. By fitting magneto-conductance at high temperature, where the WL term dominates, we can get a reliable value of B_{SO} and use it to fit the low-temperature data. Then, we only carry out a two-parameter fitting as a function of temperature. Curve fits for three characteristic samples ($x = 0.04$, 0.18, and 0.3) are shown in Figure 4a−c. WL, WAL, and the Maki−-Thompson fluctuations dominate in the temperature range of interest.

The Larkin expression for the MT term is limited to temperatures much higher than T_c and not-too-large fields ($2\pi k_B(T - T_c) \gg \hbar/\tau_\varphi$ and $2\pi k_B(T - T_c) \gg 4eDH$). This limits our fitting range of the data, especially at low temperature close to T_c. The fit parameters N and L_φ are plotted versus temperature in Figure 4d,e and L_{SO} is plotted versus x in Figure 4f. Their variation is discussed next.

The number of channels N (Figure 4d) does not exceed 3 for $x = 0.04$ and $x = 0.18$. This is expected in IV−VI materials due to their 4-fold valley degeneracy, regardless of topological character.[40,59] Despite taking into account the contribution of fluctuations, N greatly increases as the In concentration goes up. It has been suggested that In 5s states form an impurity band near the Fermi level and generate quasi-localized electrons, which gradually delocalize with increasing x.[23,38,60] Thus, In could impact valley degeneracy by altering the shape of the Fermi surface of SnTe causing N to change. However, the change could be a result of our analysis underestimating the magnitude of superconducting fluctuations, especially

https://doi.org/10.1021/acs.nanolett.1c04370
Nano Lett. XXXX, XXX, XXX−XXX

when $T_c > 3$ K. The coherence length for all samples roughly follows $L_\varphi \sim T^{-1.5}$ as shown in Figure 4e. Theoretically, in 2D inelastic electron−electron scattering leads to $L_\varphi \sim T^{-0.5}$,[61,62] while electron−phonon scattering yields a faster decay $L_\varphi \sim T^{-1.5}$ in 2D and 3D.[63−65,29] Thus, Figure 4e indicates that electron−phonon scattering is the dominant dephasing mechanism.

We further corroborate the interpretation of the quantum coherent corrections by analyzing the resistance versus temperature $R(T)$ curve of $x = 0.3$ near T_c. The detailed expression of WAL corrections and those from MT fluctuations are shown in Supporting Informaton. The $R(T)$ corrections due to other fluctuation terms can be calculated from parameters determined previously (see Supporting Information S3).[29,44,49,52−54] They yield a minimal impact at the temperatures of interest compared to the MT term. Figure 5a shows a comparison between the $R(T)$ data for $x = 0.3$ and the combined effect of the MT fluctuations and WAL, qualitatively matching the data (more details are given in Supporting Information). The MT fluctuations that lead to eq 3 are not expected to appear in measurements of the magnetization as they are related to coherent electron scattering corrections that only influence the conductivity.[66,67] Figure 5b shows the AC susceptibility χ of $Sn_{1-x}In_xTe$ ($x = 0.3$) up to 10 K at zero magnetic field. There is no visible deviation observed from background diamagnetism down to well below $T = 5$ K, despite $R(T)$ decreasing by more than 1% between 10 and 5 K. This is consistent with the MT fluctuations model. This observation also rules out the formation of superconducting clusters above T_c as they would normally produce a drop in both $R(T)$ and $\chi(T)$.

Our results thus indicate that $Sn_{1-x}In_xTe$ thin films host strong quantum coherent corrections to the conductivity, originating from the coexistence of superconducting fluctuations and partial antilocalization. We note that a strong WAL has been reported in superconducting $Sn_{1-x}In_xTe$ platelets,[68] but the corrections from superconducting fluctuations were not considered to the best of our knowledge. Properties of these fluctuations in the normal state may contain crucial information on the superconducting order parameter, as was widely studied in the cuprate superconductors.[67] Our observation and analysis of the fluctuations thus lay important groundwork for future theoretical and experimental studies on the pairing symmetry of strained $Sn_{1-x}In_xTe$. For the WAL contribution, we attribute it to bulk electrons with spin−orbit splitting instead of the Dirac surface states. This is because, on the one hand, the WAL cusp is a classical sign of strong spin−orbit interactions that reduce the backscattering probability. On the other hand, we expect the spin-momentum locking of the Dirac surface states to suppress all backscattering, which eliminates WL entirely.[69] However, we find a crossover from WAL to WL in our superconducting samples and a finite L_{SO}, indicating that carriers from spin−orbit split trivial states play a dominant role in normal state transport and possibly in the superconducting state.

This spin−orbit splitting could originate from several possible sources. In $Pb_{1-x}Sn_xSe$ quantum wells, its origin is attributed to surface inversion asymmetry that introduces a Rashba-like term in the Hamiltonian describing the system.[70] Band bending[71] introduced in a controlled way by growing quantum wells with asymmetric barriers can have a similar effect.[72] A ferroelectric crystalline distortion[73,74] that displaces the Sn and Te sublattices with respect to each other can also occur in SnTe and can yield a strong bulk Rashba splitting by breaking centrosymmetry.[75,76] We have carried out a systematic search for this distorted state using low-temperature X-ray diffraction measurements and resistivity measurements, but did not find any evidence of it in $Sn_{1-x}In_xTe$ (see Supporting Information S4).[77−80] Thus, our XRD measurements confirm the presence of rhombohedral strain but contain no evidence of the sublattice shift that breaks crystalline inversion symmetry. Hence, the precise origin of spin−orbit splitting in our samples requires further experiments.

In strongly spin−orbit-coupled systems, such as $Cu_xBi_2Se_3$, $Sn_{1-x}In_xTe$, and various transition metal dichalcogenides, parity-mixed superconductivity can naturally exist on symmetry grounds.[81−83] Odd-parity or sometimes topological superconductivity can also be energetically favored by spin−orbit coupling even when mediated by phonons.[8,83,84,81] We thus plausibly expect $Sn_{1-x}In_xTe$ thin films to host unconventional superconductivity.

In summary, we have grown $Sn_xIn_{1-x}Te$ ($0 < x < 0.3$) thin films by MBE and measured their structural, quantum coherent, and superconducting transport properties. Samples can maintain superconductivity up to 3.5 K with $x = 0.3$. In the normal state, we have observed the coexistence of superconducting fluctuations and a crossover from WAL to WL versus magnetic field. Our analysis of WAL yields a short spin−orbit scattering length consistent with strong spin−orbit splitting. The latter is a necessary but not sufficient ingredient to realize topological superconductivity. To the best of our knowledge, superconducting fluctuations have not been observed in a topological insulator that becomes superconducting. Our results thus raise several interesting questions about the superconductivity of $Sn_xIn_{1-x}Te$ thin films. First, they motivate further theoretical studies of $Sn_{1-x}In_xTe$ with the distorted crystal structure to elucidate the nature of its superconductivity. Second, they raise the question of whether superconducting fluctuations and their response to magnetic field and impurities can shed light on the pairing symmetry. At the very least, the synthesis of such thin films provides a superconducting material that one can use to grow in situ proximity effect bilayers with epitaxial interfaces based on TCIs.

■ ASSOCIATED CONTENT

Supporting Information

The Supporting Information is available free of charge at https://pubs.acs.org/doi/10.1021/acs.nanolett.1c04370.

Growth parameters and the tuning of the In concentration, results for $Sn_{0.91}In_{0.09}Te$, fitting of superconducting fluctuations, resistance ,and lattice constant versus temperature (PDF)

■ AUTHOR INFORMATION

Corresponding Authors

Jiashu Wang − *Department of Physics, University of Notre Dame, Notre Dame, Indiana 46556, United States;* Email: jwang39@nd.edu

Badih A. Assaf − *Department of Physics, University of Notre Dame, Notre Dame, Indiana 46556, United States;* orcid.org/0000-0002-6879-9651; Email: bassaf@nd.edu

https://doi.org/10.1021/acs.nanolett.1c04370
Nano Lett. XXXX, XXX, XXX−XXX

Authors

William Powers − *Department of Physics, University of Notre Dame, Notre Dame, Indiana 46556, United States*

Zhan Zhang − *X-ray Science Division, Advanced Photon Source, Argonne National Lab, Lemont, Illinois 60439, United States*

Michael Smith − *Department of Physics, University of Notre Dame, Notre Dame, Indiana 46556, United States*

Bradlee J. McIntosh − *Department of Physics, University of Notre Dame, Notre Dame, Indiana 46556, United States*

Seul Ki Bac − *Department of Physics, University of Notre Dame, Notre Dame, Indiana 46556, United States*

Logan Riney − *Department of Physics, University of Notre Dame, Notre Dame, Indiana 46556, United States*

Maksym Zhukovskyi − *Notre Dame Integrated Imaging Facility, University of Notre Dame, Notre Dame, Indiana 46556, United States*

Tatyana Orlova − *Notre Dame Integrated Imaging Facility, University of Notre Dame, Notre Dame, Indiana 46556, United States*

Leonid P. Rokhinson − *Department of Physics and Astronomy, Purdue University, West Lafayette, Indiana 47907, United States; Birck Nanotechnology Center and Department of Electrical and Computer Engineering, Purdue University, West Lafayette, Indiana 47907, United States*

Yi-Ting Hsu − *Department of Physics, University of Notre Dame, Notre Dame, Indiana 46556, United States*

Xinyu Liu − *Department of Physics, University of Notre Dame, Notre Dame, Indiana 46556, United States;* orcid.org/0000-0002-7004-6878

Complete contact information is available at: https://pubs.acs.org/10.1021/acs.nanolett.1c04370

Author Contributions

J.W. carried out X-ray diffraction, electrical measurements, and analyzed most of the data. W.P. and B.M. assisted in the electrical measurements. S.K.B. and L.R. assisted in the XRD and electrical measurements. Z.Z. carried out the low-temperature XRD measurements. M.Z. and T.O. carried out TEM measurements. X.L. grew the samples. M.S. and Y.T.H. provided theoretical insight on superconducting fluctuations and the topological character of the material. L.P.R. contributed to the interpretation of magnetotransport and susceptibility measurements. J.W., X.L., and B.A.A. conceived the project and contributed to the writing of the manuscript. X.L. and B.A.A. supervised and led the project.

Funding

Work was supported by NSF-DMR-1905277. L.P.R. acknowledges support from NSF-DMR-2005092 The Material Characterization Facility is funded by the Sustainable Energy Initiative (SEI), which is part of the Center for Sustainable Energy at Notre Dame (ND Energy). We also acknowledge support from the Notre Dame Integrated Imaging Facility. This research used resources of the Advanced Photon Source, a U.S. Department of Energy (DOE) Office of Science User Facility, operated for the DOE Office of Science by Argonne National Laboratory under Contract No. DE-AC02−06CH11357.

Notes

The authors declare no competing financial interest.

■ ACKNOWLEDGMENTS

We thank B. Janko and M. Eskildsen for useful discussions about superconducting fluctuations. We also thank Neil R. Dilley for carrying out the magnetic susceptibility measurements.

■ ABBREVIATIONS

XRD, X-ray diffraction; TEM, transmission electron microscopy; HLN, Hikami−Larkin−Nagoka; MBE, molecular beam epitaxy; TCI, topological crystalline insulator; TSC, topological superconductor; WAL, weak antilocalization; WL, weak localization; RSM, reciprocal space map; MT, Maki−Thompson

■ REFERENCES

(1) Qi, X.-L.; Zhang, S.-C. Topological Insulators and Superconductors. *Rev. Mod. Phys.* **2011**, *83* (4), 1057−1110.

(2) Hasan, M. Z.; Kane, C. L. Colloquium: Topological Insulators. *Rev. Mod. Phys.* **2010**, *82* (4), 3045−3067.

(3) Armitage, N. P.; Mele, E. J.; Vishwanath, A. Weyl and Dirac Semimetals in Three-Dimensional Solids. *Rev. Mod. Phys.* **2018**, *90* (1), No. 015001.

(4) Kitaev, A. Anyons in an Exactly Solved Model and Beyond. *Ann. Phys. (N. Y).* **2006**, *321* (1), 2−111.

(5) Sarma, S. D.; Freedman, M.; Nayak, C. Majorana Zero Modes and Topological Quantum Computation. *npj Quantum Inf.* **2015**, *1* (1), 15001.

(6) Sato, M.; Ando, Y. Topological Superconductors: A Review. *Rep. Prog. Phys.* **2017**, *80* (7), 076501.

(7) Hor, Y. S.; Williams, A. J.; Checkelsky, J. G.; Roushan, P.; Seo, J.; Xu, Q.; Zandbergen, H. W.; Yazdani, A.; Ong, N. P.; Cava, R. J. Superconductivity in CuxBi2Se3 and Its Implications for Pairing in the Undoped Topological Insulator. *Phys. Rev. Lett.* **2010**, *104* (5), 3−6.

(8) Fu, L.; Berg, E. Odd-Parity Topological Superconductors: Theory and Application to CuxBi2Se3. *Phys. Rev. Lett.* **2010**, *105* (9), No. 097001.

(9) Ran, S.; Eckberg, C.; Ding, Q. P.; Furukawa, Y.; Metz, T.; Saha, S. R.; Liu, I. L.; Zic, M.; Kim, H.; Paglione, J.; Butch, N. P. Nearly Ferromagnetic Spin-Triplet Superconductivity. *Science (80-.).* **2019**, *365* (6454), 684−687.

(10) Avers, K. E.; Gannon, W. J.; Kuhn, S. J.; Halperin, W. P.; Sauls, J. A.; DeBeer-Schmitt, L.; Dewhurst, C. D.; Gavilano, J.; Nagy, G.; Gasser, U.; Eskildsen, M. R. Broken Time-Reversal Symmetry in the Topological Superconductor UPt3. *Nat. Phys.* **2020**, *16* (5), 531−535.

(11) Fu, L.; Kane, C. L. Superconducting Proximity Effect and Majorana Fermions at the Surface of a Topological Insulator. *Phys. Rev. Lett.* **2008**, *100* (9), 1−4.

(12) Bocquillon, E.; Deacon, R. S.; Wiedenmann, J.; Leubner, P.; Klapwijk, T. M.; Brüne, C.; Ishibashi, K.; Buhmann, H.; Molenkamp, L. W. Gapless Andreev Bound States in the Quantum Spin Hall Insulator HgTe. *Nat. Nanotechnol.* **2017**, *12*, 137.

(13) Trimble, C. J.; Wei, M. T.; Yuan, N. F. Q.; Kalantre, S. S.; Liu, P.; Han, H.-J.; Han, M.-G.; Zhu, Y.; Cha, J. J.; Fu, L.; Williams, J. R. Josephson Detection of Time-Reversal Symmetry Broken Superconductivity in SnTe Nanowires. *npj Quantum Mater.* **2021**, *6* (1), 61.

(14) Snyder, R. A.; Trimble, C. J.; Rong, C. C.; Folkes, P. A.; Taylor, P. J.; Williams, J. R. Weak-Link Josephson Junctions Made from Topological Crystalline Insulators. *Phys. Rev. Lett.* **2018**, *121* (9), No. 097701.

(15) Tanaka, Y.; Ren, Z.; Sato, T.; Nakayama, K.; Souma, S.; Takahashi, T.; Segawa, K.; Ando, Y. Experimental Realization of a Topological Crystalline Insulator in SnTe. *Nat. Phys.* **2012**, *8* (11), 800−803.

(16) Hsieh, T. H.; Lin, H.; Liu, J.; Duan, W.; Bansil, A.; Fu, L. Topological Crystalline Insulators in the SnTe Material Class. *Nat. Commun.* **2012**, *3*, 982.

https://doi.org/10.1021/acs.nanolett.1c04370
Nano Lett. XXXX, XXX, XXX−XXX

(17) Tanaka, Y.; Shoman, T.; Nakayama, K.; Souma, S.; Sato, T.; Takahashi, T.; Novak, M.; Segawa, K.; Ando, Y. Two Types of Dirac-Cone Surface States on the (111) Surface of the Topological Crystalline Insulator SnTe. *Phys. Rev. B - Condens. Matter Mater. Phys.* **2013**, *88*, 235216.
(18) Polley, C. M.; Dziawa, P.; Reszka, A.; Szczerbakow, A.; Minikayev, R.; Domagala, J. Z.; Safaei, S.; Kacman, P.; Buczko, R.; Adell, J.; Berntsen, M. H.; Wojek, B. M.; Tjernberg, O.; Kowalski, B. J.; Story, T.; Balasubramanian, T. Observation of Topological Crystalline Insulator Surface States on (111)-Oriented Pb 1-x Sn x Se Films. *Phys. Rev. B - Condens. Matter Mater. Phys.* **2014**, *89*, No. 075317.
(19) Erickson, A. S.; Chu, J.-H.; Toney, M. F.; Geballe, T. H.; Fisher, I. R. Enhanced Superconducting Pairing Interaction in Indium-Doped Tin Telluride. *Phys. Rev. B* **2009**, *79* (2), No. 024520.
(20) Si, W.; Zhang, C.; Wu, L.; Ozaki, T.; Gu, G.; Li, Q. Superconducting Thin Films of (100) and (111) Oriented Indium Doped Topological Crystalline Insulator SnTe. *Appl. Phys. Lett.* **2015**, *107* (9), No. 092601.
(21) Balakrishnan, G.; Bawden, L.; Cavendish, S.; Lees, M. R. Superconducting Properties of the In-Substituted Topological Crystalline Insulator SnTe. *Phys. Rev. B* **2013**, *87* (14), 140507.
(22) Bliesener, A.; Feng, J.; Taskin, A. A.; Ando, Y. Superconductivity in Sn1-XInxTe Thin Films Grown by Molecular Beam Epitaxy. *Phys. Rev. Mater.* **2019**, *3* (10), 101201.
(23) Haldolaarachchige, N.; Gibson, Q.; Xie, W.; Nielsen, M. B.; Kushwaha, S.; Cava, R. J. Anomalous Composition Dependence of the Superconductivity in In-Doped SnTe. *Phys. Rev. B* **2016**, *93* (2), No. 024520.
(24) Maeda, S.; Hirose, R.; Matano, K.; Novak, M.; Ando, Y.; Zheng, G. Spin-Singlet Superconductivity in the Doped Topological Crystalline Insulator Sn0.96In0.04Te. *Phys. Rev. B* **2017**, *96* (10), 104502.
(25) Smylie, M. P.; Claus, H.; Kwok, W.-K.; Louden, E. R.; Eskildsen, M. R.; Sefat, A. S.; Zhong, R. D.; Schneeloch, J.; Gu, G. D.; Bokari, E.; Niraula, P. M.; Kayani, A.; Dewhurst, C. D.; Snezhko, A.; Welp, U. Superconductivity, Pairing Symmetry, and Disorder in the Doped Topological Insulator Sn1-XInxTe for X > 0.1. *Phys. Rev. B* **2018**, *97* (2), No. 024511.
(26) Nomoto, T.; Kawamura, M.; Koretsune, T.; Arita, R.; Machida, T.; Hanaguri, T.; Kriener, M.; Taguchi, Y.; Tokura, Y. Microscopic Characterization of the Superconducting Gap Function in Sn1-x InxTe. *Phys. Rev. B* **2020**, *101* (1), 14505.
(27) Smylie, M. P.; Kobayashi, K.; Takahashi, T.; Chaparro, C.; Snezhko, A.; Kwok, W.-K.; Welp, U. Nodeless Superconducting Gap in the Candidate Topological Superconductor < math> < msub> < mi Mathvariant = ″normal″>Sn</Mi> < mrow> < mn > 1</Mn> < mo>−</Mo> < mi > x</Mi> < /Mrow> < /Msub> < msub> < mi Mathvariant = ″normal″>In</Mi> < mi > x</Mi> < /Msub> < mi Mathvariant = ″nor. *Phys. Rev. B* **2020**, *101* (9), No. 094513.
(28) Du, G.; Du, Z.; Fang, D.; Yang, H.; Zhong, R. D.; Schneeloch, J.; Gu, G. D.; Wen, H.-H. Fully Gapped Superconductivity in In-Doped Topological Crystalline Insulator Pb0.5Sn0.5Te. *Phys. Rev. B* **2015**, *92* (2), No. 020512.
(29) Bergmann, G. Weak Localization in Thin Films: A Time-of-Flight Experiment with Conduction Electrons. *Phys. Rep.* **1984**, *107*, 1.
(30) Larkin, A. Reluctance of Two-Dimensional Systems. *JETP Lett.* **1980**, *31* (4), 219−223.
(31) Sacépé, B.; Chapelier, C.; Baturina, T. I.; Vinokur, V. M.; Baklanov, M. R.; Sanquer, M. Pseudogap in a Thin Film of a Conventional Superconductor. *Nat. Commun.* **2010**, *1* (1), 140.
(32) Carretta, P.; Livanov, D. V.; Rigamonti, A.; Varlamov, A. A. Superconducting Fluctuations and 63Cu NQR-NMR Relaxation in YBa2Cu3O7-δ Effect of Magnetic Field and a Test for the Pairing-State Symmetry. *Phys. Rev. B* **1996**, *54* (14), R9682−R9685.
(33) Mitrovic, V. F.; Bachman, H. N.; Halperin, W. P.; Eschrig, M.; Sauls, J. A.; Reyes, A. P.; Kuhns, P.; Moulton, W. G. Superconducting Fluctuation Effects on the Spin-Lattice Relaxation Rate in YBa2Cu3O6.95. *Phys. Rev. Lett.* **1999**, *82* (13), 2784−2787.
(34) Masuko, M.; Yoshimi, R.; Tsukazaki, A.; Kawamura, M.; Takahashi, K. S.; Kawasaki, M.; Tokura, Y. Molecular Beam Epitaxy of Superconducting Sn1-XInxTe Thin Films. *Phys. Rev. Mater.* **2020**, *4* (9), No. 091202.
(35) Zhong, R. D.; Schneeloch, J. A.; Shi, X. Y.; Xu, Z. J.; Zhang, C.; Tranquada, J. M.; Li, Q.; Gu, G. D. Optimizing the Superconducting Transition Temperature and Upper Critical Field of Sn1-XInxTe. *Phys. Rev. B* **2013**, *88* (2), No. 020505.
(36) Zhong, R.; He, X.; Schneeloch, J. A.; Zhang, C.; Liu, T.; Pletikosić, I.; Yilmaz, T.; Sinkovic, B.; Li, Q.; Ku, W.; Valla, T.; Tranquada, J. M.; Gu, G. Surface-State-Dominated Transport in Crystals of the Topological Crystalline Insulator In-Doped Pb1-XSnxTe. *Phys. Rev. B* **2015**, *91* (19), 195321.
(37) Novak, M.; Sasaki, S.; Kriener, M.; Segawa, K.; Ando, Y. Unusual Nature of Fully Gapped Superconductivity in In-Doped SnTe. *Phys. Rev. B* **2013**, *88* (14), 140502.
(38) Zhang, C.; He, X.-G.; Chi, H.; Zhong, R.; Ku, W.; Gu, G.; Tranquada, J. M.; Li, Q. Electron and Hole Contributions to Normal-State Transport in the Superconducting System Sn1-XInxTe. *Phys. Rev. B* **2018**, *98* (5), No. 054503.
(39) Hikami, S.; Larkin, A. I.; Nagaoka, Y. Spin-Orbit Interaction and Magnetoresistance in the Two Dimensional Random System. *Prog. Theor. Phys.* **1980**, *63* (2), 707−710.
(40) Peres, M. L.; Monteiro, H. S.; Chitta, V. a.; de Castro, S.; Mengui, U. a.; Rappl, P. H. O.; Oliveira, N. F.; Abramof, E.; Maude, D. K. Experimental Investigation of Spin-Orbit Coupling in n-Type PbTe Quantum Wells. *J. Appl. Phys.* **2014**, *115* (9), No. 093704.
(41) Assaf, B. A.; Katmis, F.; Wei, P.; Satpati, B.; Zhang, Z.; Bennett, S. P.; Harris, V. G.; Moodera, J. S.; Heiman, D. Quantum Coherent Transport in SnTe Topological Crystalline Insulator Thin Films. *Appl. Phys. Lett.* **2014**, *105* (10), 102108.
(42) Akiyama, R.; Fujisawa, K.; Yamaguchi, T.; Ishikawa, R.; Kuroda, S. Two-Dimensional Quantum Transport of Multivalley (111) Surface State in Topological Crystalline Insulator SnTe Thin Films. *Nano Res.* **2016**, *9* (2), 490−498.
(43) Zhang, C.; Liu, Y.; Yuan, X.; Wang, W.; Liang, S.; Xiu, F. Highly Tunable Berry Phase and Ambipolar Field Effect in Topological Crystalline Insulator Pb(1-x)Sn(x)Se. *Nano Lett.* **2015**, *15* (3), 2161−2167.
(44) Wang, J.; Liu, X.; Bunker, C.; Riney, L.; Qing, B.; Bac, S. K.; Zhukovskyi, M.; Orlova, T.; Rouvimov, S.; Dobrowolska, M.; Furdyna, J. K.; Assaf, B. A. Weak Antilocalization beyond the Fully Diffusive Regime in Pb1-XSnxSe Topological Quantum Wells. *Phys. Rev. B* **2020**, *102* (15), 155307.
(45) Aslamasov, L. G.; Larkin, A. I. The Influence of Fluctuation Pairing of Electrons on the Conductivity of Normal Metal. *Phys. Lett. A* **1968**, *26* (6), 238−239.
(46) Redi, M. H. Tvvo-Dimensional Fluctuation-Induced Conductivity above the Critical Temperatures. *Phys. Rev. B* **1977**, *16* (5), 2027.
(47) Thompson, R. S. Microwave, Flux Flow, and Fluctuation Resistance of Dirty Type-II Superconductors. *Phys. Rev. B* **1970**, *1* (1), 327−333.
(48) Maki, K. Critical Fluctuation of the Order Parameter in a Superconductor. *I. Prog. Theor. Phys.* **1968**, *40* (2), 193−200.
(49) Dorin, V. V.; Klemm, R. A.; Varlamov, A. A.; Buzdin, A. I.; Livanov, D. V. Fluctuation Conductivity of Layered Superconductors in a Perpendicular Magnetic Field. *Phys. Rev. B* **1993**, *48* (17), 12951−12965.
(50) Ioffe, L. B.; Larkin, A. I.; Varlamov, A. A.; Yu, L. Effect of Superconducting Fluctuations on the Transverse Resistance of High-Tc Superconductors. *Phys. Rev. B* **1993**, *47* (14), 8936−8941.
(51) Nakamura, H.; Huang, D.; Merz, J.; Khalaf, E.; Ostrovsky, P.; Yaresko, A.; Samal, D.; Takagi, H. Robust Weak Antilocalization Due to Spin-Orbital Entanglement in Dirac Material Sr3SnO. *Nat. Commun.* **2020**, *11* (1), 1161.

https://doi.org/10.1021/acs.nanolett.1c04370
Nano Lett. XXXX, XXX, XXX−XXX

(52) Larkin, A.; Varlamov, A. *Theory of Fluctuations in Superconductors*; Oxford University Press, 2005.
(53) Altshuler, B. L.; Aronov, A. G. Electron−Electron Interaction In Disordered Conductors. In *Modern Problems in Condensed Matter Sciences*; Elsevier, 1985; Vol. *10*, pp 1−153.
(54) Lopes dos Santos, J. M. B.; Abrahams, E. Superconducting Fluctuation Conductivity in a Magnetic Field in Two Dimensions. *Phys. Rev. B* **1985**, *31* (1), 172−176.
(55) Larkin, A. I.; Varlamov, A. A. Fluctuation Phenomena in Superconductors. In *Superconductivity*; Springer Berlin Heidelberg: Berlin, Heidelberg, 1997; pp 369−458.
(56) Bergmann, G. Quantum Corrections to the Resistance in Two-Dimensional Disordered Superconductors above Tc: Al, Sn, and Amorphous Bi0.9Tl0.1 Films. *Phys. Rev. B* **1984**, *29* (11), 6114−6128.
(57) Giannouri, M.; Rocofyllou, E.; Papastaikoudis, C.; Schilling, W. Weak-Localization, Aslamazov-Larkin, and Maki-Thompson Superconducting Fluctuation Effects in Disordered Films Above. *Phys. Rev. B - Condens. Matter Mater. Phys.* **1997**, *56* (10), 6148−6156.
(58) Harris, D. T.; Campbell, N.; Uecker, R.; Brützam, M.; Schlom, D. G.; Levchenko, A.; Rzchowski, M. S.; Eom, C.-B. Superconductivity-Localization Interplay and Fluctuation Magnetoresistance in Epitaxial BaPb1-XBixO3. *Phys. Rev. Mater.* **2018**, *2* (4), No. 041801.
(59) Bishop, D. J.; Dynes, R. C.; Tsui, D. C. Magnetoresistance in Si Metal-Oxide-Semiconductor Field-Effect Transitors: Evidence of Weak Localization and Correlation. *Phys. Rev. B* **1982**, *26* (2), 773−779.
(60) Maeda, S.; Katsube, S.; Zheng, G.-Q. Quasi-Localized Impurity State in Doped Topological Crystalline Insulator Sn 0.9 In 0.1 Te Probed by 125 Te-NMR. *J. Phys. Soc. Jpn.* **2017**, *86* (2), No. 024702.
(61) Altshuler, B. L.; Aronov, A. G.; Khmelnitsky, D. E. Effects of Electron-Electron Collisions with Small Energy Transfers on Quantum Localisation. *J. Phys. C Solid State Phys.* **1982**, *15* (36), 7367−7386.
(62) Abrahams, E.; Anderson, P. W.; Lee, P. A.; Ramakrishnan, T. V. Quasiparticle Lifetime in Disordered Two-Dimensional Metals. *Phys. Rev. B* **1981**, *24* (12), 6783−6789.
(63) Raffy, H.; Nedellec, P.; Dumoulin, L.; MacLachlan, D. S.; Burger, J. P. ANOMALOUS MAGNETORESISTANCE IN 2D Pd AND PdHx FILMS. *J. Phys. Paris* **1985**, *46* (4), 627−635.
(64) Lin, J. J.; Bird, J. P. Recent Experimental Studies of Electron Dephasing in Metal and Semiconductor Mesoscopic Structures. *J. Phys.: Condens. Matter* **2002**, *14* (18), R501.
(65) Belitz, D.; Das Sarma, S. Inelastic Phase-Coherence Time in Thin Metal Films. *Phys. Rev. B* **1987**, *36* (14), 7701−7704.
(66) Kasahara, S.; Yamashita, T.; Shi, A.; Kobayashi, R.; Shimoyama, Y.; Watashige, T.; Ishida, K.; Terashima, T.; Wolf, T.; Hardy, F.; Meingast, C.; Löhneysen, H. V.; Levchenko, A.; Shibauchi, T.; Matsuda, Y. Giant Superconducting Fluctuations in the Compensated Semimetal FeSe at the BCS−BEC Crossover. *Nat. Commun.* **2016**, *7* (1), 12843.
(67) Varlamov, A. A.; Balestrino, G.; Milani, E.; Livanov, D. V. The Role of Density of States Fluctuations in the Normal State Properties of High Tc Superconductors. *Adv. Phys.* **1999**, *48* (6), 655−783.
(68) Shen, J.; Xie, Y.; Cha, J. J. Revealing Surface States in In-Doped SnTe Nanoplates with Low Bulk Mobility. *Nano Lett.* **2015**, *15* (6), 3827−3832.
(69) Lu, H. Z.; Shi, J.; Shen, S. Q. Competition between Weak Localization and Antilocalization in Topological Surface States. *Phys. Rev. Lett.* **2011**, *107* (7), 1−5.
(70) Kazakov, A.; Brzezicki, W.; Hyart, T.; Turowski, B.; Polaczyński, J.; Adamus, Z.; Aleszkiewicz, M.; Wojciechowski, T.; Domagala, J. Z.; Caha, O.; Varykhalov, A.; Springholz, G.; Wojtowicz, T.; Volobuev, V. V.; Dietl, T. Signatures of Dephasing by Mirror-Symmetry Breaking in Weak-Antilocalization Magnetoresistance across the Topological Transition in Pb1-XSnxSe. *Phys. Rev. B* **2021**, *103* (24), 245307.
(71) Volobuev, V. V.; Mandal, P. S.; Galicka, M.; Caha, O.; Sánchez-Barriga, J.; Di Sante, D.; Varykhalov, A.; Khiar, A.; Picozzi, S.; Bauer, G.; Kacman, P.; Buczko, R.; Rader, O.; Springholz, G. Giant Rashba Splitting in Pb 1- x Sn x Te (111) Topological Crystalline Insulator Films Controlled by Bi Doping in the Bulk. *Adv. Mater.* **2017**, *29* (3), 1604185.
(72) Hasegawa, M. M.; de Andrada e Silva, E. A. Spin-Orbit-Split Subbands in IV-VI Asymmetric Quantum Wells. *Phys. Rev. B* **2003**, *68* (20), 205309.
(73) Brillson, L. J.; Burstein, E.; Muldawer, L. Raman Observation of the Ferroelectric Phase in SnTe. *Phys. Rev. B* **1974**, *9* (4), 1547−1551.
(74) Chang, K.; Kaloni, T. P.; Lin, H.; Bedoya-Pinto, A.; Pandeya, A. K.; Kostanovskiy, I.; Zhao, K.; Zhong, Y.; Hu, X.; Xue, Q.; Chen, X.; Ji, S.; Barraza-Lopez, S.; Parkin, S. S. P. Enhanced Spontaneous Polarization in Ultrathin SnTe Films with Layered Antipolar Structure. *Adv. Mater.* **2019**, *31* (3), 1804428.
(75) Bangert, E.; Bauer, G.; Fantner, E. J.; Pascher, H. Magneto-Optical Investigations of Phase-Transition-Induced Band-Structure Changes of Pb1-XGexTe. *Phys. Rev. B* **1985**, *31* (12), 7958−7978.
(76) Plekhanov, E.; Barone, P.; Di Sante, D.; Picozzi, S. Engineering Relativistic Effects in Ferroelectric SnTe. *Phys. Rev. B* **2014**, *90* (16), 161108.
(77) Takaoka, S.; Murase, K. Anomalous Resistivity near the Ferroelectric Phase Transition in (Pb, Ge, Sn)Te Alloy Semiconductors. *Phys. Rev. B* **1979**, *20* (7), 2823−2833.
(78) Fan, H; Grassie, A D C Resistivity Anomaly and Phase Transition of Pb 1-x Ge x Se. *J. Phys. C Solid State Phys.* **1985**, *18* (21), 4121−4125.
(79) Iizumi, M.; Hamaguchi, Y.; Komatsubara, K. F.; Kato, Y. Phase Transition in SnTe with Low Carrier Concentration. *J. Phys. Soc. Jpn.* **1975**, *38* (2), 443−449.
(80) Clemens, H.; Ofner, P.; Krenn, H.; Bauer, G. Epitaxial Growth of Pb1−xGexTe Films and of PbTe/Pb1−xGexTe Superlattices. *J. Cryst. Growth* **1987**, *84* (4), 571−576.
(81) Yuan, N. F. Q.; Mak, K. F.; Law, K. T. Possible Topological Superconducting Phases of MoS2. *Phys. Rev. Lett.* **2014**, *113* (9), No. 097001.
(82) Sohn, E.; Xi, X.; He, W.-Y.; Jiang, S.; Wang, Z.; Kang, K.; Park, J.-H.; Berger, H.; Forró, L.; Law, K. T.; Shan, J.; Mak, K. F. An Unusual Continuous Paramagnetic-Limited Superconducting Phase Transition in 2D NbSe 2. *Nat. Mater.* **2018**, *17* (6), 504−508.
(83) Hsu, Y.-T.; Vaezi, A.; Fischer, M. H.; Kim, E.-A. Topological Superconductivity in Monolayer Transition Metal Dichalcogenides. *Nat. Commun.* **2017**, *8* (1), 14985.
(84) Brydon, P. M. R.; Das Sarma, S.; Hui, H.-Y.; Sau, J. D. Odd-Parity Superconductivity from Phonon-Mediated Pairing: Application to CuxBi2Se3. *Phys. Rev. B* **2014**, *90* (18), 184512.

https://doi.org/10.1021/acs.nanolett.1c04370
Nano Lett. XXXX, XXX, XXX−XXX